Wave Basin Testing and Numerical Analysis of a Very Light FOWT with Guy-wires

Conference Paper · October 2018

DOI: 10.17648/sobena-2018-87611

CITATIONS
0

READS
68

8 authors, including:

Lucas Henrique Souza do Carmo
University of São Paulo
6 PUBLICATIONS **2** CITATIONS
SEE PROFILE

Daniel Prata Vieira
University of São Paulo
18 PUBLICATIONS **13** CITATIONS
SEE PROFILE

Edgard Malta
University of São Paulo
22 PUBLICATIONS **60** CITATIONS
SEE PROFILE

Pedro Cardozo de Mello
University of São Paulo
30 PUBLICATIONS **38** CITATIONS
SEE PROFILE

27º Congresso Internacional de Transporte Aquaviário, Construção Naval e Offshore

Rio de Janeiro/RJ, 23-25 de outubro de 2018

Wave Basin Testing and Numerical Analysis of a Very Light FOWT with Guy-wires

Lucas H. S. do Carmo, Escola Politécnica/USP, São Paulo/Brazil, lucas.carmo@usp.br
Daniel P. Vieira, Technomar Engenharia Oceânica, São Paulo/Brazil
Jiang Xiong, School of Frontier Sciences/University of Tokyo, Tokyo/Japan
Edgard B. Malta, Technomar Engenharia Oceânica, São Paulo/Brazil
Alexandre N. Simos, Escola Politécnica/USP, São Paulo/Brazil
Pedro C. Mello, Escola Politécnica/USP, São Paulo/Brazil
Hideyuki Suzuki, Dept. of Systems Innovation/University of Tokyo, Tokyo/Japan
Rodolfo T. Gonçalves, Dept. of Systems Innovation/University of Tokyo, Tokyo/Japan

Abstract

The floater structure is responsible for one of the main costs of a floating offshore wind turbine (FOWT), leading to a large effort to reducing its structural weight in new designs. In this context, this paper describes the concept of a very light semi-submersible floater consisting of a central column, which sustains the tower, connected by pontoons to three equally spaced columns. The central column is connected by guy-wires to the top of the offset columns, allowing for a light structure.

In order to investigate the performance of this FOWT concept, an experimental campaign of a 1/80th scale model was performed in a wave basin. As the FOWT is structurally light, both pontoons and guy-wires are subject to the effects of hydroelasticity. Only waves were considered, thus wind effects are not addressed. The main results are the tension at the guy wires, the strain at selected positions on the pontoons, and the first order motions of the FOWT. The motions are compared with numerical simulations performed with the software NK-UTWind, METiS-USP, and WAMIT.

1. Introduction

Wind energy has shown an impressive growth over the last 20 years (Global Wind Energy Council, 2018). Most of the installed capacity is located onshore, but since areas with steady and strong winds are a scarce resource, locations that meet the conditions necessary for the installation of new wind farms are increasingly rare. This is especially true for countries that have been harnessing wind energy for several years and/or are small in terms of area, such as several European countries (Portugal, UK, Denmark, France, among others) and Japan.

These circumstances led to the idea of installing wind turbines at sea, taking advantage of the large availability of area with winds that are very often stronger and steadier than those found onshore. These offshore wind turbines can be fixed to the seabed, a viable solution in water depths up to around 50 m, or installed on top of floating platforms, allowing the structure to be deployed in deeper waters. By the end of 2017, the global offshore wind capacity was around 19 GW, mostly due to fixed foundation offshore wind farms. Several prototypes of floating offshore wind turbines (FOWT) have been installed around the world since the first one by Blue H in 2007 (Huber, 2008), while the first floating offshore wind farm, Equinor's Hywind Scotland, began production in October 2017 (Equinor, 2018).

The analysis and design of a FOWT must take into account the hydrodynamics of the floater, the dynamics of the mooring system, aerodynamics and controls of the turbine, elasticity of the structure, and the complex environmental conditions due to wind, waves and current. The development of simulation software that could

accurately reproduce those effects has been the focus of several works, since these tools are important to the design of FOWTs. Among these works, the OC4 (Robertson, et al., 2014) and OC5 (Robertson, et al., 2017) projects are especially relevant for including a very large number of participants and comparing several different modeling approaches. Concerning model tests, Stewart and Muskulus (2016) presents a recent review of the ones carried out so far, with additional examples provided by Li et 2018, Martin (2011), and Shin et at (2013).

The present work discusses the results of an experimental campaign of a 1/80th scale model FOWT in a wave basin. The structure consists of a very-light semi-submersible floater consisting of a central column, which sustains the tower, connectd by pontoons to three equally spaced columns. The central column is connect by guy-wires to the top of the offset columns, allowing for a light structure. As the FOWT is very light, its structure is subject to hydroelastic effects, specially the pontoons and the guy wires. At this stage of the work, only wave effects were considered.

Besides analysing the hydroeslastic behaviour of the structure, the experimental campaign is also useful for validating the numerical software under development at the University of Tokyo (NK-UTWind) and at the University of São Paulo (METiS-USP). Therefore, the main results are the tension at the guy wires, the strain at selected positions on the pontoons, and the first order motions of the FOWT. The motions are compared with numerical simulations performed with the two software under development and with WAMIT, a commercial Boundary Element Method code for analyzing the interaction of offshore structures with waves.

2. Experimental setup

The model tests were conducted in the Hydrodynamic Calibrator of the University of São Paulo (USP), illustrated in Figure 1, a squared wave basin with dimensions 14 m x 14 m 4 m equipped with 148 active-absorber wave generators. It is able to generate the waves and to absorb the waves diffracted and radiated by the model, following specific control algorithms. The wave peak period ranges between 0.8 s and 2.5 s in model scale. In order to achieve the intended peak periods in the experiments, the model tests were conducted in 1/80th scale.

The construction of the model took into account the geometry of the FOWT, the flexural rigidity of the vertical tower and of the pontoons, and the hydrostatic and hydrodynamic behavior of the floater, as summarized in Tables Table 1 and Table 2. One should notice that the natural periods of roll and pitch are the same, a consequence of the symmetry of the model.

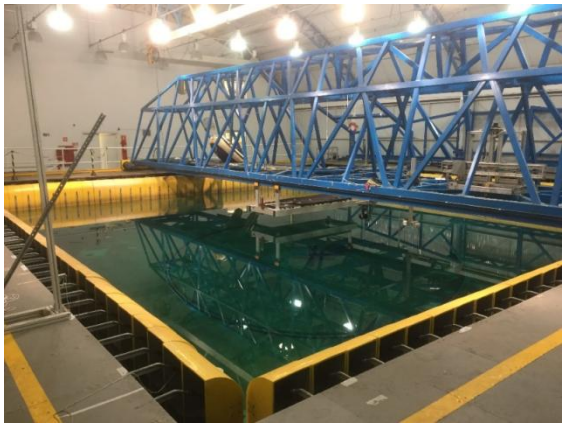

Figure 1: USP wave basin

The guy wires were made of stained steel cables with non-scaled stiffness. The pontoons and the tower were modeled by steel core beams designed to match the scaled flexural rigidity (EI) of the prototype. In order to achieve the geometry and buoyancy of the pontoons, six segmented blocks of urethane foam covered their core beams. The hydrostatic characteristics were verified by free decay tests, while the flexural rigidities of the tower and of the pontoons were calculated based on the geometry and material of the core beams.

Table 1: Prototype and model main dimensions

	Dimension	Prototype	Exp. Model (1/80)
Tower	Diameter	7 *m*	87.5 *mm*
	Height	105 *m*	1312.5 *mm*
Columns	Diameter	7 *m*	87.5 *mm*
	Height	25 *m*	312.5 *mm*
Pontoons	Length	30 *m*	375 *mm*
	Height	5 *m*	62.5 *mm*
	Width	7 *m*	87.5 *mm*

The four columns were modeled by cylinders made of fiberglass and urethane. The lower part of each side column had a ballast to calibrate the vertical center of gravity and inertia. Figures Figure 2 and Figure 3 show the experimental model described above. The center of gravity (CoG) of the model defines the center of the model coordinate system, with the X axis along one of the pontoons, the Z axis upwards, and the Y axis given by the right-hand rule. The guy-wires connect the junctions between columns and pontoons to the top of the tower, and they were pre-tensioned in such a way that they did not slacken during the tests.

Table 2: Main hydrostatic and structural characteristics of the FOWT

Item	Prototype	Exp. Model(1/80)
Displacement	5774 *ton*	11.25 *kg*
KB	4.59 *m*	57.48 *mm*
BM	16.08 *m*	201.46 *mm*
KG	8.31 *m*	104.64 *mm*
GM	12.36 *m*	154.30 *mm*
T_n Heave	16.6 *s*	1.86 *s*
T_n Roll/Pitch	20.6 *s*	2.28 *s*
EI Pontoon	$2.707 \cdot 10^{11}\ Pa \cdot m^4$	$8.26 \cdot 10^{1}\ Pa \cdot m^4$
EI Tower	$5.031 \cdot 10^{11}\ Pa \cdot m^4$	$1.54 \cdot 10^{2}\ Pa \cdot m^4$

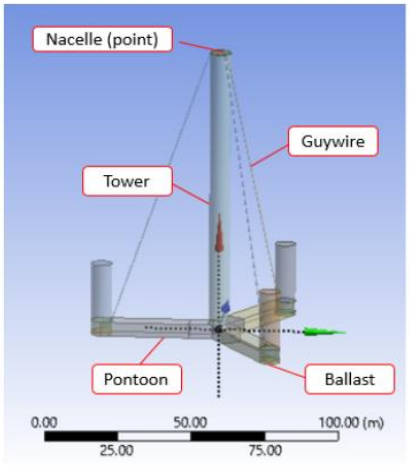

Figure 2: Prototype overview

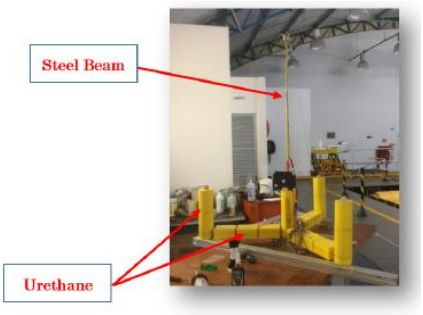

Figure 3: Experimental model

The model motions were measured using Qualisys optical tracking system. In order to obtain accuracy and redundancy to the motion measurement, four tracking cameras with five passive markers on the base of the tower were used, leading to a marker position error of less than 1.0 mm. The sample frequency for measuring the motions was 100 Hz.
The bending of the pontoon cores and of the tower core were measured using strain gauges located at selected points, as shown in Figure 4. The points FP denote the gauges located in the pontoons at a radial distance of 135 mm and 272 mm of the center of the model, while FC are the points at the center tower core aligned to each pontoon and located 100 mm above the model bottom. These gauges were calibrated in straing (μS). The points FG are the locations of the gauges used to measure the tension at the guy wires, calibrated in Newtons (N).

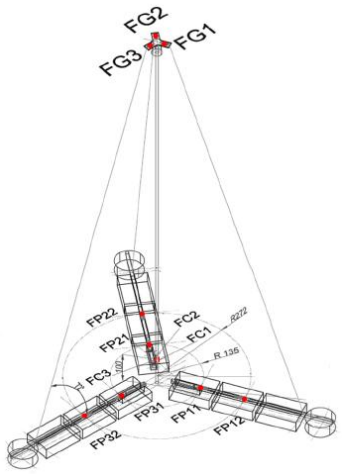

Figure 4: Location of strain gauges

Due to the symmetry of the FOWT, which presents an angle between pontoons of 120°, a heading sweep of 60° covers all wave incidences of interest. Hence, the wave incidences analyzed in the experiments were 180° (head seas), 195°, 210°, 225°, and 240°. The model was moored using three horizontal anchoring lines attached to each of the offset columns. In the end of each line there is a spring connected to the borders of the wave basin, with a stiffness of 2.2 N/m and a pre-tension of 0.49 N (in full scale, these values correspond to 14 kN/m and 252 kN). The different headings are achieved by fixing the other end of the mooring lines to different positions at the border of the wave basin, as illustrated in Figure 5. A set of three wave probes was used to measure the waves during the experiment, and an additional wave probe was positioned at the model location during the phase of wave calibration.

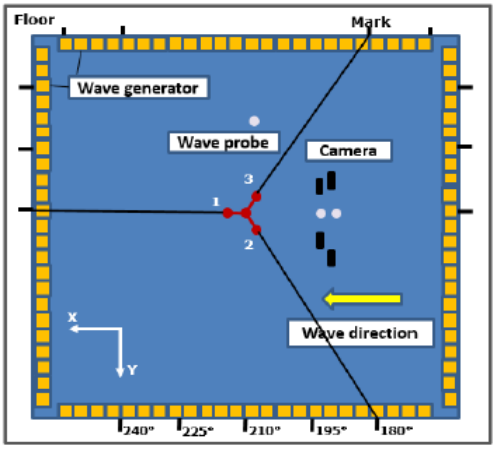

Figure 5: Top view of the wave basin

Four types of waves were analyzed in the experiment. Transient and white noise waves provided a rapid RAO evaluation, and they were devised in such a way that they covered the whole range of periods of interest using low wave elevation in linear condition. Three irregular waves, modeled by the JONSWAP spectrum, were employed to study the behavior of the model in typical seas. For the headings of 180°, 210° and 240°, a set of regular waves was made covering a range of periods of operation cases. The characteristic of the waves analyzed are provided in Tables Table 3, Table 4 and Table 5.

Table 3: Regular wave characteristics

WAVE ID	Prototype		Model	
	T_p (s)	H_s (m)	T_p (s)	H_s (mm)
FOWT-REG01	16.350	0.5	1.83	6.25
FOWT-REG02	16.350	1.0	1.83	12.5
FOWT-REG03	16.350	2.0	1.83	25
FOWT-REG04	16.350	4.0	1.83	50
FOWT-REG05	16.350	5.0	1.83	62.5
FOWT-REG06	16.350	6.0	1.83	75
FOWT-REG07	6.000	3.0	0.67	37.5
FOWT-REG08	7.000	3.0	0.78	37.5
FOWT-REG09	8.000	3.0	0.89	37.5
FOWT-REG10	9.000	3.0	1.00	37.5
FOWT-REG11	10.000	3.0	1.12	37.5
FOWT-REG12	11.000	3.0	1.23	37.5
FOWT-REG13	12.000	3.0	1.34	37.5
FOWT-REG14	13.000	3.0	1.45	37.5
FOWT-REG15	14.000	3.0	1.57	37.5
FOWT-REG16	15.000	3.0	1.68	37.5
FOWT-REG17	16.000	3.0	1.79	37.5
FOWT-REG18	17.000	3.0	1.90	37.5

Table 4: White noise wave characteristics

WAVE ID	Wave Characteristics (Prototype)				Wave Characteristics (Model)			
	T_p^{min} (s)	T_p^{max} (s)	H_s (m)	Duration (h)	T_p^{min} (s)	T_p^{max} (s)	H_s (mm)	Duration (s)
FOWT-WHI01	6.6	17.9	2	0.50	0.74	2.00	25.00	200

Table 5: Irregular wave characteristics

WAVE ID	TYPE	Wave Characteristics (Prototype)			Wave Characteristics (Model)		
		H_s (m)	T_p (s)	Duration (h)	H_s (mm)	T_p (s)	Duration (s)
FOWT-IRR01	JONSWAP	2.5	9.0	3.0	31.6	1.006	1207
FOWT-IRR02	JONSWAP	9.8	13.5	3.0	122.5	1.509	1207
FOWT-IRR03	JONSWAP	4.0	16.1	3.0	50.6	1.800	1207

3. Numerical models

Besides the experiments, the motions of the FOWT were calculated using the following software:

1. METiS-USP, an in-house code for the analysis of floating systems with little diffraction, such as floating offshore wind turbines, currently under development at the University of Sao Paulo. Since it is in an early phase of development, the first order motions calculated by the other software and the ones measured in the experiment are an important way of validating the code;
2. NK-UTWind, a software for the coupled analysis of floating offshore wind turbines, developed by ClassNK and the University of Tokyo. Both METiS-USP and NK-UTWind employ Morison's equation for calculating the hydrodynamic loads;
3. WAMIT, a commercial Boundary Element Method code for analyzing wave interactions with offshore structures, which evaluates the hydrodynamics loads through the solution of the radiation/diffraction problem in frequency domain. As it is based in a different hydrodynamic method than both NK-UTWind and METiS-USP, simulations with WAMIT are useful to highlight the conditions in which each method is better at reproducing the experimental results.
4.

Details about how the FOWT is modeled in each of the software are provided below, as well as a brief explanation of the part of the theory behind NK-UTWind and METiS-USP that is most relevant for this work.

3.1. WAMIT

The WAMIT simulation was conducted with a higher order mesh composed of 30 patches. In this method, the geometry of the body is described by B-sploes and all quantities are continuous inside each panel (details can be found in WAMIT, Inc., 2013). After a convergence analysis, the panel size parameter was set to 4. An illustration of the mesh is given in Figure 6.

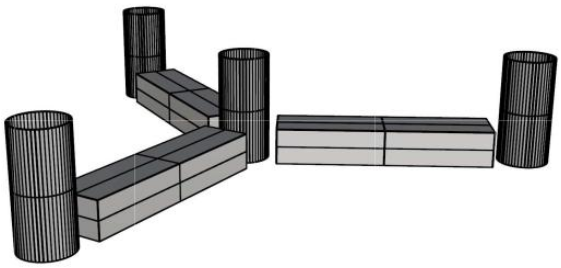

Figure 6: Higher order mesh used in the WAMIT simulations

Since WAMIT is a potential theory code, it is necessary to include additional damping terms to (partially) account for viscous damping, especially for the motions in the vertical directions (heave, roll, and pitch), in order to avoid spurious amplifications around the resonance frequency of each degree of freedom. Based on results from previous works and on the author's experience, an additional damping of 5% of the critical damping is a good estimation (see, for example, Simos, Ruggeri, Watai, Souto-Iglesias, and Lopez-Pavon, 2018 for a discussion on the damping coefficient of semi-submersible FOWTs).

3.2. METiS-USP

As stated above, METiS-USP is an in-house code under development at the University of Sao Paulo for the time domain analysis of floating systems with little diffraction. The structure is considered as a rigid body comprised of slender circular and rectangular cylinders, in such a way that the application of Morison's equation for the calculation of hydrodynamics forces yields good results. Besides, as cylinders are very simple geometric shapes, the calculation of the displaced volume and of the center of volume is very straightforward, meaning that the hydrostatic force can be easily calculated at each time step.

Adopting a local coordinate system *Oxyz* for each cylinder, with the origin *O* at the base of the cylinder, *z* the axial direction, and *x* and *y* the two axes of symmetry of a rectangular cylinder (or two arbitrary axes for a circular cylinder), the forces acting at each section are given by:

$$\begin{bmatrix} dF_x \\ dF_y \end{bmatrix} = \rho A \begin{bmatrix} (1 + \dot{C}_{ax})\,\dot{u}_x \\ (1 + \dot{C}_{ay})\,\dot{u}_y \end{bmatrix} - \rho A \begin{bmatrix} C_{ax}\ddot{q}_x \\ C_{ay}\ddot{q}_y \end{bmatrix} + \frac{1}{2}\rho \left|\vec{u}_p - \dot{\vec{q}}_p\right| \begin{bmatrix} D_y C_{Dx}(u_x - \dot{q}_x) \\ D_x C_{Dy}(u_y - \dot{q}_y) \end{bmatrix} \quad (1)$$

Where ρ is the fluid density, A is the cross sectional area, $\vec{u}_p = u_x\vec{e}_x + u_y\vec{e}_y$ is the component of the fluid velocity that is perpendicular to the cylinder axis, and $\vec{q}_p = q_x\vec{e}_x + q_y\vec{e}_y$ is the component of the cylinder displacement, calculated at that specific section, that is perpendicular to the cylinder. D_x and D_y are the width (or diameter) of the cylinder, C_{ax} and C_{ay} the added mass coefficients in *x* and *y* direction, and C_{Dx} and C_{Dy} the drag coefficients in *x* and *y* direction. The total force acting at each cylinder is obtained by integrating the infinitesimal forces calculated at a certain number of nodes along its length using Simpson's rule. The nodes position of each cylinder is updated at each time step for the evaluation of the hydrodynamic loads.

In the axial direction, the force is calculated using the following equation:

$$F_z = \frac{1}{2}\rho C_{Dz} A\,|u_z\,\dot{q}_z\,|(u_z - \dot{q}_z) + \rho C_{az} V_R(\dot{u}_z - \ddot{q}_z) + p_b S_b - p_t S_t \quad (2)$$

With $V_R = \frac{4}{3}\pi\left(\frac{D_x + D_y}{2}\right)^3$; p_b and p_t the dynamic pressure, due only toe the undisturbed incoming wave, at the bottom and at the top of the column, and S_b and S_t the surface of the bottom and top faces of the column. The term $p_t S_t$ is non-zero only when the column is submerged, such as when modeling heave plates.

For the FOWT studied in this work, the drag and added mass coefficients of the pontoons were determined from the results presented by Venugopal, Varyani, and Barltrop (2006), while the drag coefficient of the columns was calculated with the results from Catalano, Wang, Iaccarino, and Moin (2003). As both the drag and added mass coefficients depend on the Keulegan-Carpenter and Reynolds number, na average value was taken for all the wave conditions, and care was taken to keep the resulting added mass in surge and heave close to the ones obtained with WAMIT. For the added mass coefficient of the columns, the value calculated with potential theory was adopted. The axial drag coefficient of both the pontoons nad the columns was considered to be zero, as it must be negligile face the drag due to the other elements. The resulting coefficients are provided in Table 6. For the pontoons, *x* is the horizontal direction and *y* is the vertical.

Table 6: Added mass and drag coefficients adopted in METiS-USP

Coefficient	Columns	Pontoons
C_{Dx}	0.7	4.0
C_{Dy}	0.7	5.0
C_{Dz}	0.0	0.0
C_{ax}	1.00	0.65
C_{ay}	1.00	1.20
C_{az}	0.80	0.00

For calculating the fluid velocity, the waves are modeled following linear theory (Airy wave) with no stretching. For now, the restoration due to the mooring system is modeled as a linear stiffness matrix. The aerodynamic loads on the blades is under development

3.3. NK-UTWind

NK-UTWind is a software for the coupled analysis of floating offshore wind turbines. In a complete FOWT modeling, the blades and the floater are modeled as frames structures with beam elements. The mooring lines are described according to lumped mass model, while the aerodynamic load

on the blades is computed using Blade Element Momentum Theory. A complete description of the theory implemented in NK-UTWind can be found in Suzuki, Shibata, Fujioka, Hirabayashi, Ishii, and Kikuchi (2013). For the present work, the most relevant part of NK-UTWind theory is the calculation of the hydrodynamic load.

As most FOWTs are comprised of slender structural elements, such as cylinders, NK-UTWind employs Morison elements for the evaluation of hydrostatic restoration and hydrodynamic loading (see Eq. 1). The restoring force is computed at each time step by summing the hydrostatic pressure on each element at the instantaneous position, while the hydrodynamic force is calculated using Morison's equation. Wheeler's strech method is used to estimate the wave velocity field, and the instantaneous wave load is evaluated considering submergence of each structural element.

The added mass and drag coefficients adopted in the NK-UTWind simulation are given in Table 7.

Table 7: Added mass and drag coefficients adopted in NK-UTWind

Coefficient	Columns	Pontoons
C_{Dx}	1.0	1.0
C_{Dy}	1.0	1.0
C_{Dz}	0.0	0.0
C_{ax}	1.00	1.00
C_{ay}	1.00	1.00
C_{az}	0.80	0.80

Although in this work only the first order motions are calculated with NK-UTWind, an objective for the near future is to calculate the tensions at the guy wires and the strain at the tower bottom and at the pontoons with the software, using the experimental results for validation.

4. Results

This section compares the first order motion RAOs calculated by the three different software with the ones provided by the experiments, followed by a discussion of the hydroelastic behavior observed in the experimental tests. The motion RAOs are useful for validating the software and indicating the wave conditions in which they are reliable, while the hydroelastic results bring interesting conclusions by themselves. Since many experimental results were obtained, they are provided in the Annex A.

4.1. Motion RAOs

Figure 7 to Figure 10 present the motion RAOs (Response Amplitude Operators) measured in the experiment and the ones calculated with the three different software for a wave direction of 210°. From the experimental campaign, only the results for the regular waves and for the white-noise wave are shown, as the other waves yielded similar RAOs. The wave direction of 210° was chosen to illustrate the response of the floater because all the degrees of freedom show significant motion. Besides, the conclusions are the same that can be drawn from the other wave directions. Finally, given the symmetry of the floater, the behavior in surge/sway and in roll/pitch is the same (for the same wave direction, of course, and only qualitatively for roll and pitch). Hence, only the RAOs of surge, heave, pitch, and yaw are presented.

In surge (or sway), both WAMIT and NK-UTWind agree very well with the experimental results. METiS-USP, however, shows a significant difference for longer wave periods, with the maximum relative error equal to approximately 24% when the wave direction is 180°. The difference between NK-UTWind and METiS-USP may be due to the different coefficients employed and/or to the adoption of wave stretching.

For the heave motion, all the results show a good adherence in general. The main exception is around 15.6 s, where WAMIT is not able to reproduce the experimental result, which was already expected due to the motion being caused by viscous effects. Moreover, NK-UTWind underestimates the motion for wave periods between 12s and 17s.

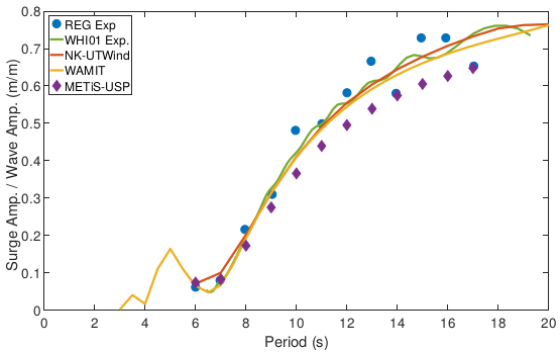

Figure 7: Surge motion comparison between the experiment and numerical simulations for a wave direction equal to 210°

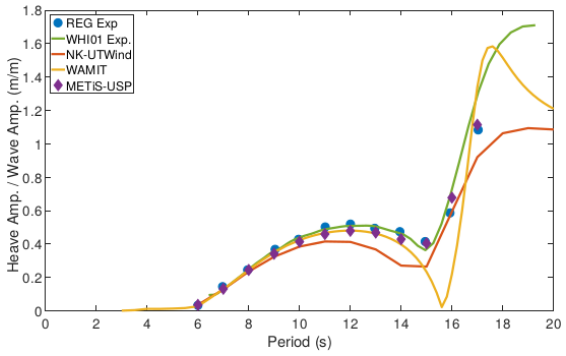

Figure 8: Heave motion comparison between the experiment and numerical simulations for a wave direction equal to 210°

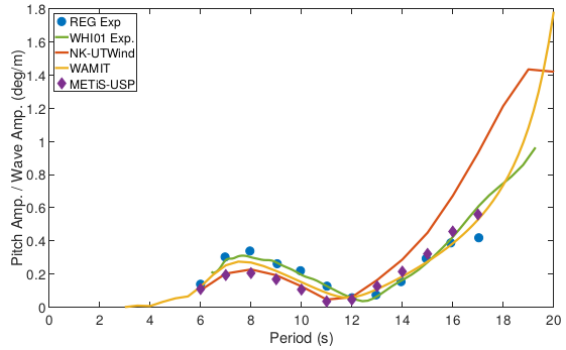

Figure 9: Pitch motion comparison between the experiment and numerical simulations for a wave direction equal to 210°

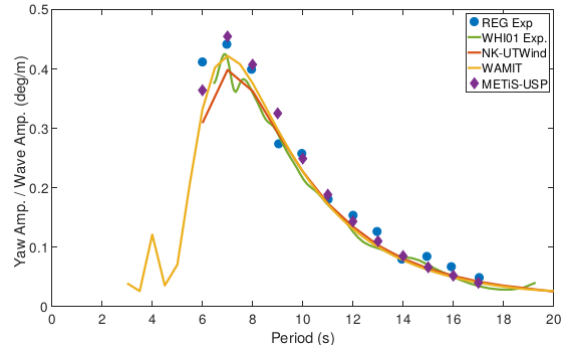

Figure 10: Yaw motion comparison between the experiment and numerical simulations for a wave direction equal to 210°

In pitch (or roll), NK-UTWind and METiS-USP agree well between each other for short waves, and they both underestimate the motion measured in the experiments. This may be due to diffraction effects, which become more relevant as the wave gets shorter. Although large in relative terms (the worst case is around 70% for T=11s, when NK-UTWind and METiS-USP predict a nearly null motion), they are small in absolute terms, as the maximum difference is around 0.13° for T=7s. For longer waves, METiS-USP agrees well with the experiment, while NK-UTWind provides larger amplitudes.

Finally, all the results in yaw are very similar, with no significant aspect worth mentioning.

4.2. Tension at guy-wires and strain at selected locations

The hydroelastic results obtained during the experimental campaign are given in the Annex A.

Due to the cancellation of the pitch motion (around 12 s), which coincides with a wavelength approximately twice the outside diameter of the platform, the acceleration in the RNA reduces, reducing the flexural stress in the central column. Likewise, the tension in the guy wires reduces as well. In pontoons, the force remains constant. In the natural heave period, all the twelve sensors measure a large force due to the large heave motion.

A force peak occurs in all tests on all twelve sensors near 6.6 s. This is the period for which the wavelength is equal to the distance between columns projected in the wave direction, In this condition, the floater is sagging/hogging, resulting in large forces on the hull. In this situation, two wave peaks are passing through the side columns while the central column is near the wave trough (the opposite occurs half a wave period later).

In a nutshell, there are 3 observed effects:

1. Amplification of all forces in the natural heave period;
2. Cancellation at the wave period that corresponds to the minimum combination of pitch and heave motions, related to a wavelength close to twice the platform diameter;
3. Amplification of the forces when the wavelength is equal to the diameter of the platform, i.e. when the hull is sagging/hogging.

5. Conclusion

This work presented the results of an experimental campaign of the floater of a very-light semi-submersible FOWT. The floater consists of a central column, which sustains the tower, connected by pontoons to three offset columns. The tower is connected by guy wires to the offset columns. The main results were the first order motions, the tension at the guy wires, the tower bottom strain, and the strain at selected positions on the pontoons. The motion RAOs were compared with

the ones calculated by three different software: NK-UTWind, METiS-USP and WAMIT.

The measured motions were useful mainly for validating the software, besides shedding light on some aspects of the hydroelastic behavior of the floater. The motions obtained showed a good general agreement, and details can be found in the text.

About the hydroelastic results, it is worth mentioning that the deformation of the guy wires is as combination of the deformation of the tower and the pontoons. Since both the tower and the pontoons are largely affect by the pitch motions, it is possible to say that the tension variation at the guy wires is dominated by pitch. Hence, the cancellation of the pitch motion around 12 s (which corresponds to a wavelength of approximately twice the outside diameter of the platform) reduces the acceleration of the RNA, leading to a corresponding reduction of the tower bottom strain and on the tension at the guy wires. In the pontoons, the stress remains constant for a large rang of wave periods.

At the heave natural period, all the twelve sensors measured large efforts, due to the large heave motion. Besides, all the sensors measured a force peak at a wave period around 6.6 s, and this behavior was observed in all tests. This period corresponds to a wavelength equal to the distance between columns projected in the wave direction, meaning that the floater is sagging/hogging, causing large loads on the hull. To summarize, three main hydroelastic effects were observed:

I. Amplification of all forces in the natural heave period;
II. Minimum loads at the wave period for which the combined heave and pitch motions are minimum, which is observed for a wavelength around twice the platform diameter. In this condition, the tension at the guy wires may be zero, depending on the wave incidence;
III. Amplification of the forces when the wavelength is equal to the diameter of the platform (sagging/hogging).

6. Acknowledgment

The authors would like to thank the technical team of the Numerical Offshore Tank – USP for their help during the model tests. Lucas Henrique Souza do Carmo acknowledges CAPES, the Brazilian Federal Agency for Post-Graduate Education, for his PhD grant. Jiang Xiong would like to acknowledge The Japan Society of Naval Architects and Ocean Engineers (JASNAOE) for the financial support of his internship period in Brazil when the model was tested. Alexandre Simos acknowledges CNPq, the Brazilian National Council for Scientific and Technological Development, for his research grant.

7. References

Catalano, P., Wang, M., Iaccarino, G., & Moin, P. (2003). Numerical simulation of the flow around a circular cylinder at high Reynolds number. *International Journal of Heat and Fluid Flow , 24*, 463-469.

Chodnekar, Y. P., Mandal, S., & Rao, B. (2015). Hydrodynamic analysis of floating offshore wind turbine. *Procedia Engineering , 116*, 4-11.

de Mello, P., Carneiro, M., Tannuri, E., Kassab, F., Marques, R., Adamowski, J., et al. (2013). A control and automation system for wave basins. *Mechatronics , 23* (1), 94-107.

Equinor. (2018). Retrieved Aug. 15, 2018, from Equinor's website: https://www.equinor.com/en/what-we-do/hywind-where-the-wind-takes-us.html#ambition

Global Wind Energy Council. (2018). *Global Wind Report: annual market update 2017.* Brussels.

Huber, F. (2008). The first floating wind turbines. *2nd International Conference on Ocean Energy (ICOE2008)* .

Li, L., Gao, Y., Hu, Z., Yuan, Z., Day, S., & Li, H. (2018). Model test research of a semisubmersible floating wind turbine with an improved deficient thrust force correction approach. *Renewable Energy , 119*, 95-105.

Martin, H. R. (2011). Development of a scale model wind turbine for testing of offshore floating wind turbine systems. : Master's thesis, University of Maine, US.

Nielsen, F. G., Hanson, T. D., & Skaare, B. (2006). Integrated dynamic analysis of floating offshore wind turbines. *25th International Conference on Offshore Mechanics and Arctic Engineering, American Society of Mechanical Engineers (OMAE2006)* , 671-679.

Robertson, A., Jonkman, J., Vorpahl, F., Popko, W., Qvist, J., Froyd, L., et al. (2014). Offshore Code

Comparison Collaboration, Continuation within IEA Wind Task 30: Phase II Results Regarding a Floating Semisubmersible Wind System. *33rd International Conference on Offshore Mechanics and Arctic Engineering, American Society of Mechanical Engineers (OMAE2014)* .

Robertson, A., Wendt, F., Jonkman, J. M., Popko, W., Dagher, H., Gueydon, S., et al. (2017). OC5 Project Phase II: Validation of Global Loads of the DeepCwind Floating Semisubmersible Wind Turbine. *Energy Procedia , 137*, 38-57.

Shin, H., Dam, P. T., Jung, K. J., Song, J., Rim, C., & Chung, T. (2013). Model test of new floating offshore wind turbines platforms. *International Journal of Naval Architects , 5* (2), 199-209.

Simos, A. N., Ruggeri, F., Watai, R. A., Souto-Iglesias, A., & Lopez-Pavon, C. (2018). Slow-drift of a floating wind turbine: An assessment of frequency-domain methods based on model tests. *Renewable Energy , 116* (4), 133-154.

Stewart, G., & Muskulus, M. (2016). A review and comparison of floating offshore wind turbine model experiments. *Energy Procedia , 94*, 227-231.

Suzuki, H., Shibata, H., Fujioka, H., Hirabayashi, S., Ishii, K., & Kikuchi, H. (2013). Development of an analysis code of rotor-floater coupled response of a floating offshore widn turbine. *32nd International Conference on Offshore Mechanics and Arctic Engineering, American Society of Mechanical Engineers (OMAE2013)* .

Venugopal, V., Varyani, K. S., & Barltrop, N. D. (2006). Wave force coefficients for horizontally submerged rectangular cylinders. *Ocean Engineering , 33*, 1669-1704.

WAMIT, Inc. (2013). *WAMIT User Manual, Version 7.0.*

Wang, C., Utsunomiya, T., Wee, S., & Choo, Y. (2010). Research on floating wind turbines: a literature survey. *The IES Journal Part A: Civil & Structural Engineering , 3* (4), 267-277.

Annex A. Experimental results

This section presents all the main results obtained in the experimental campaign. The results regarding the tension at the guy wires, strain at the tower, and strain at select points of the pontoons are presented following the nomenclature introduced in Section 2.

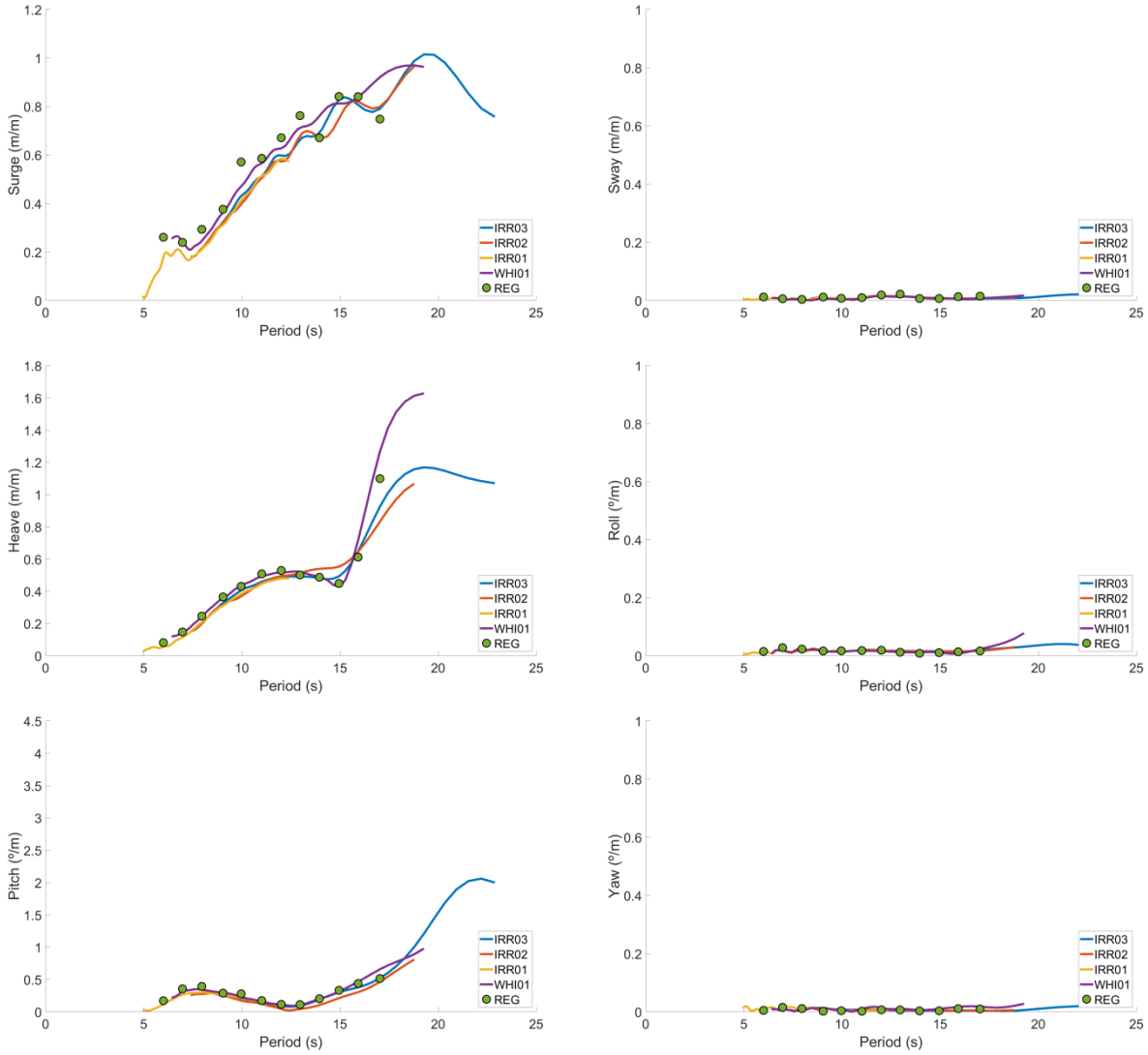

Figure 11: Motions measured in the experiments for a wave direction equal to 180°

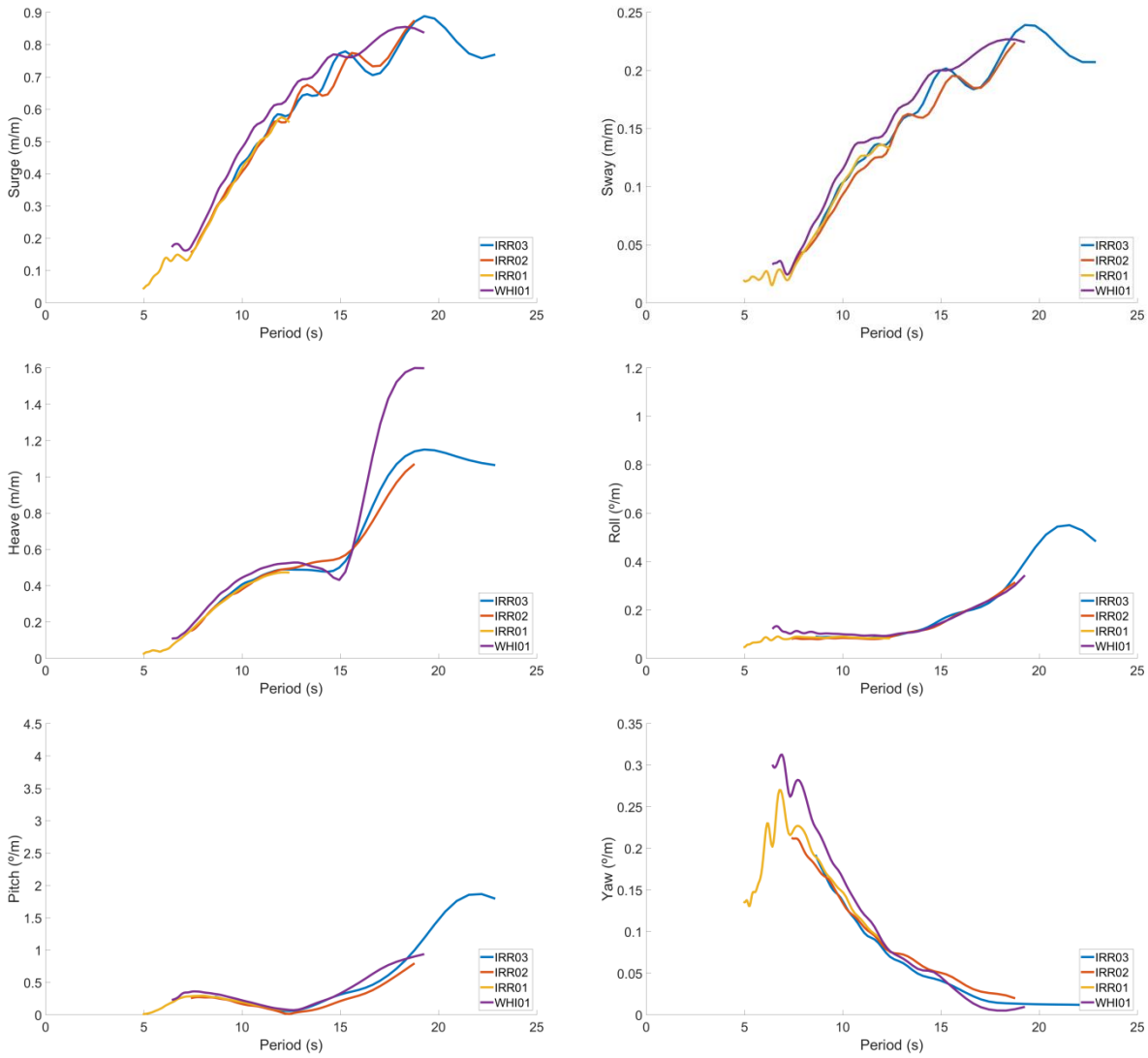

Figure 12: Motions measured in the experiments for a wave direction equal to 195°

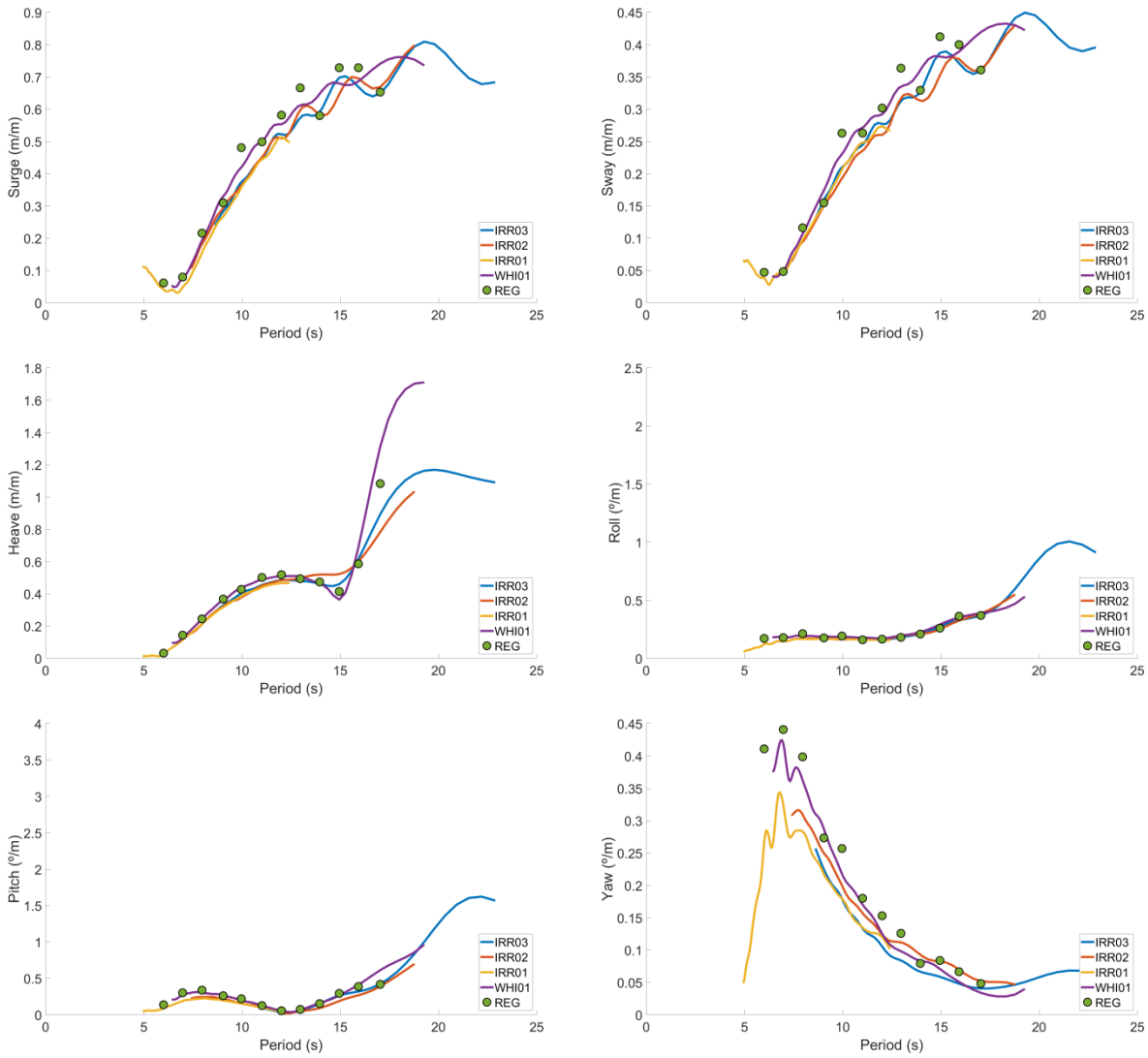

Figure 13: Motions measured in the experiments for a wave direction equal to 210°

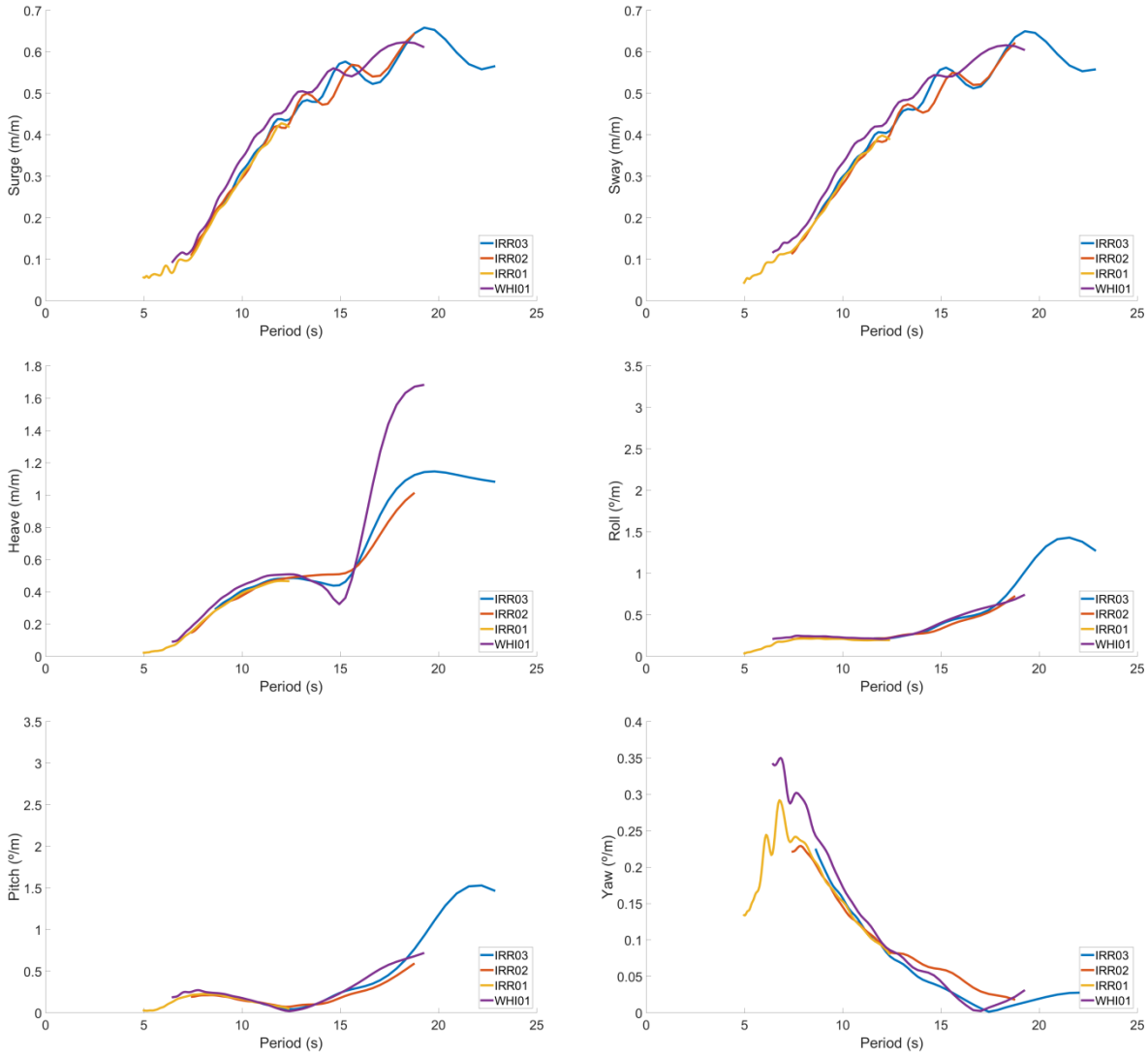

Figure 14: Motions measured in the experiments for a wave direction equal to 225°

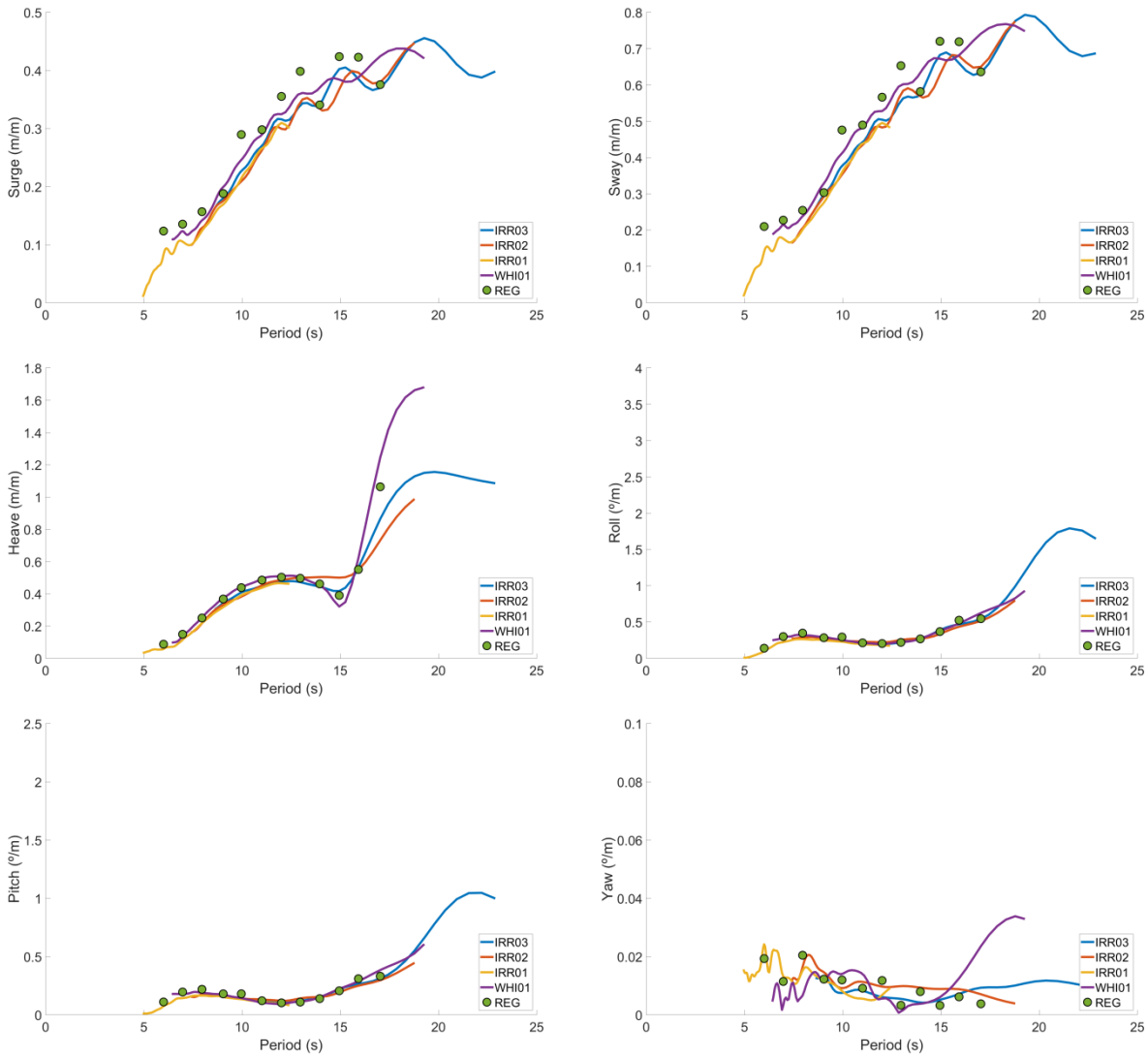

Figure 15: Motions measured in the experiments for a wave direction equal to 240°

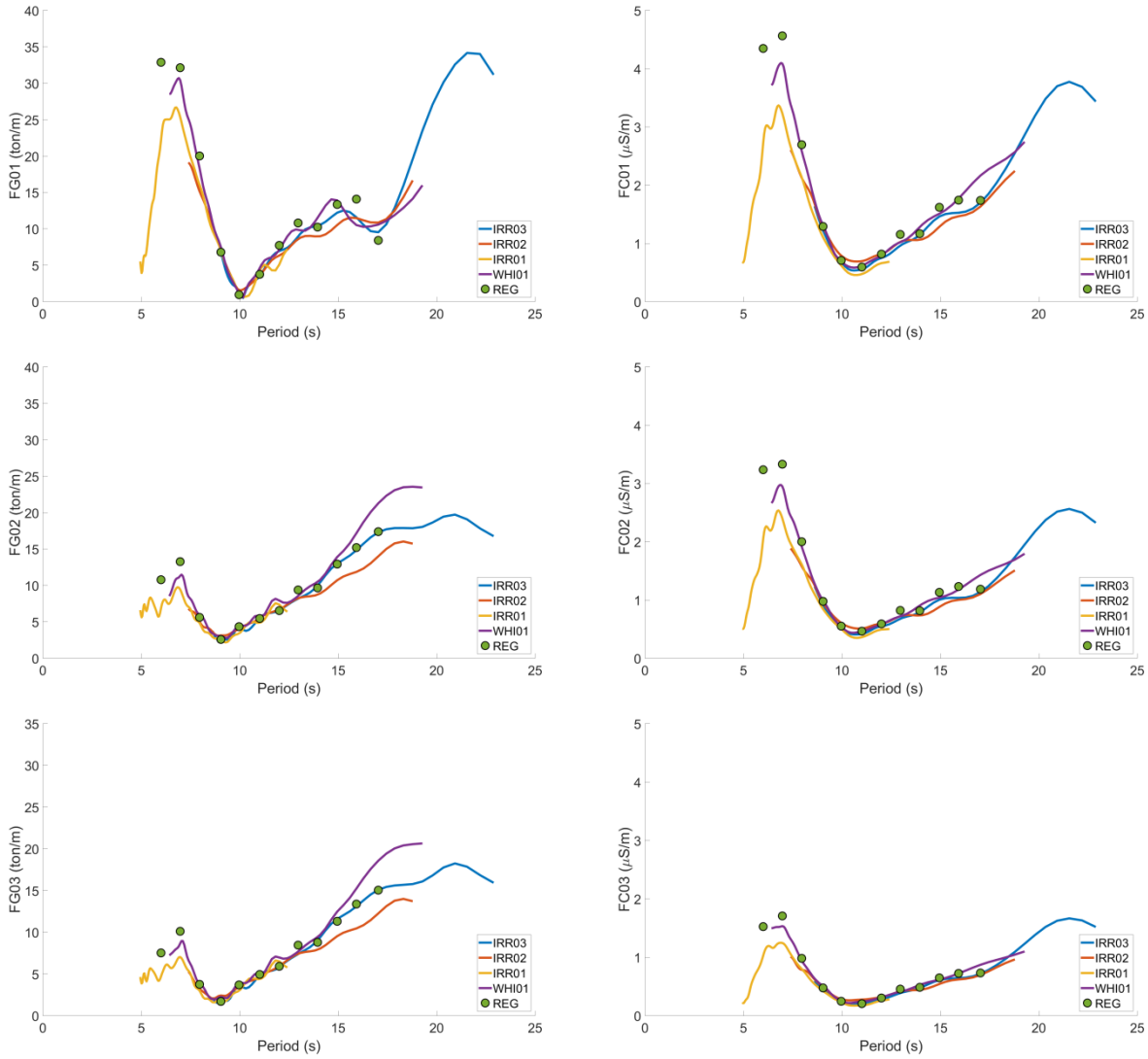

Figure 16: Tension at guy wires and tower bottom strain for a wave direction of 180°

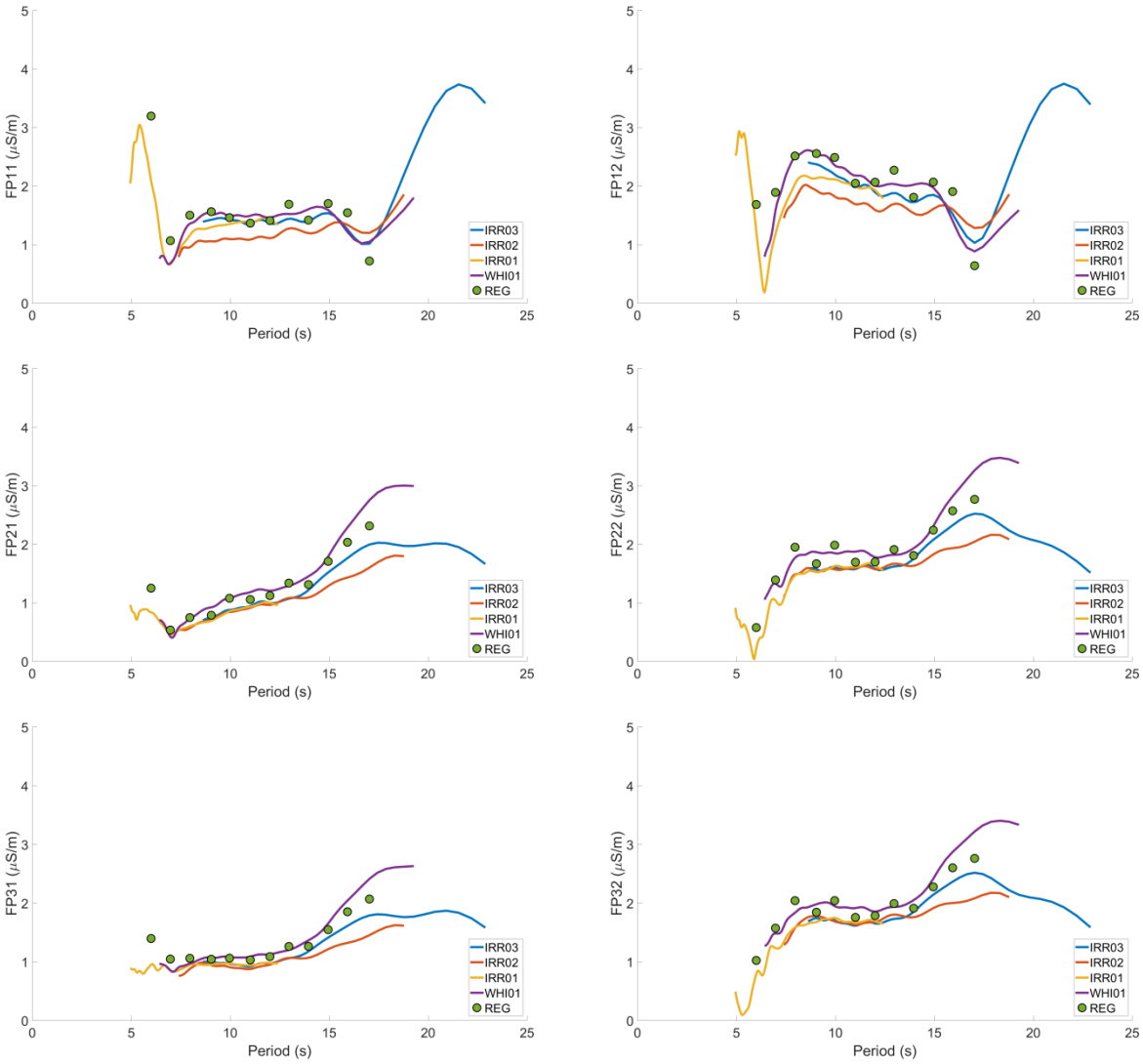

Figure 17: Strain at the selected points of the pontoons for a wave direction of 180°

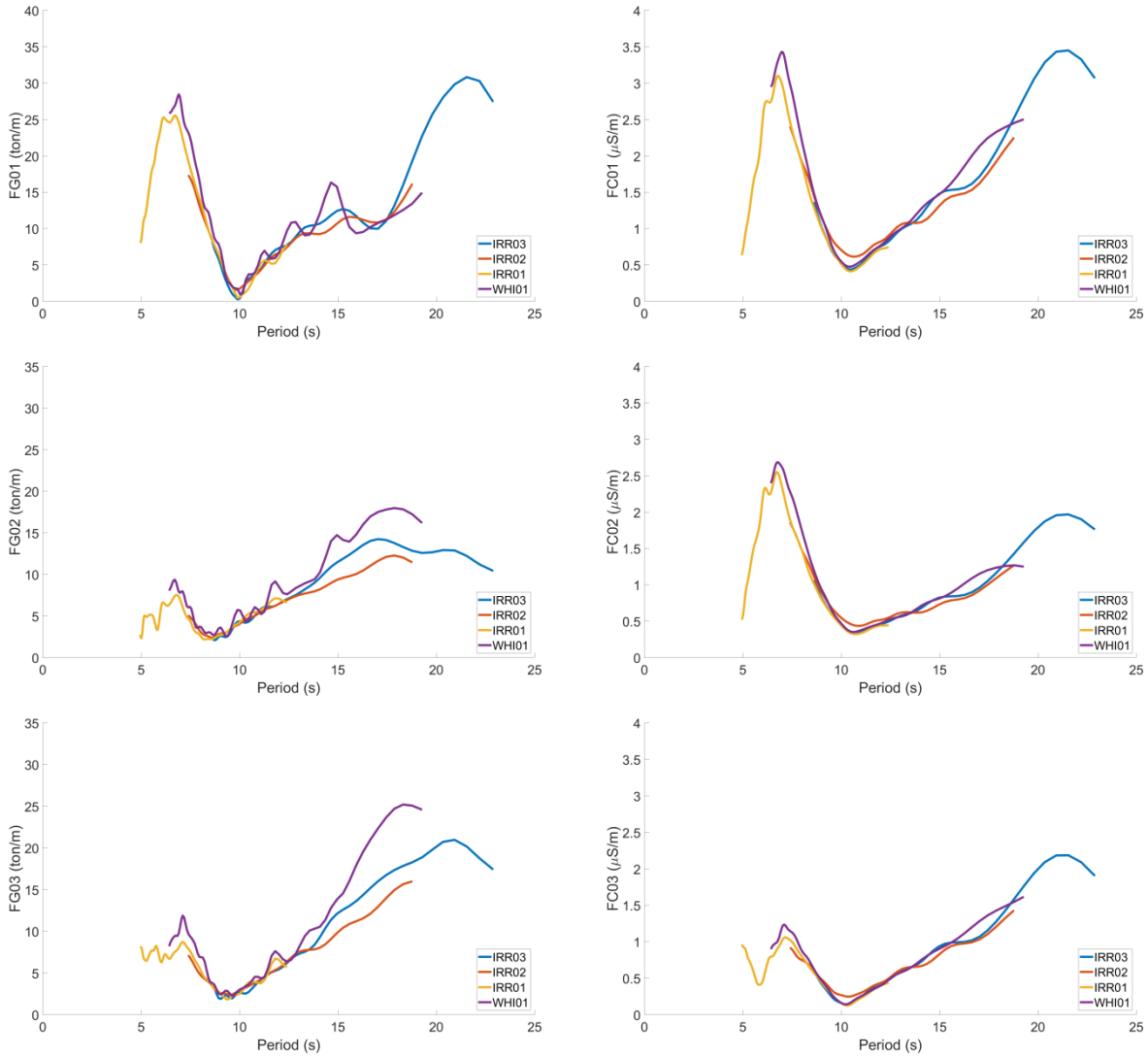

Figure 18: Tension at guy wires and tower bottom strain for a wave direction of 195°

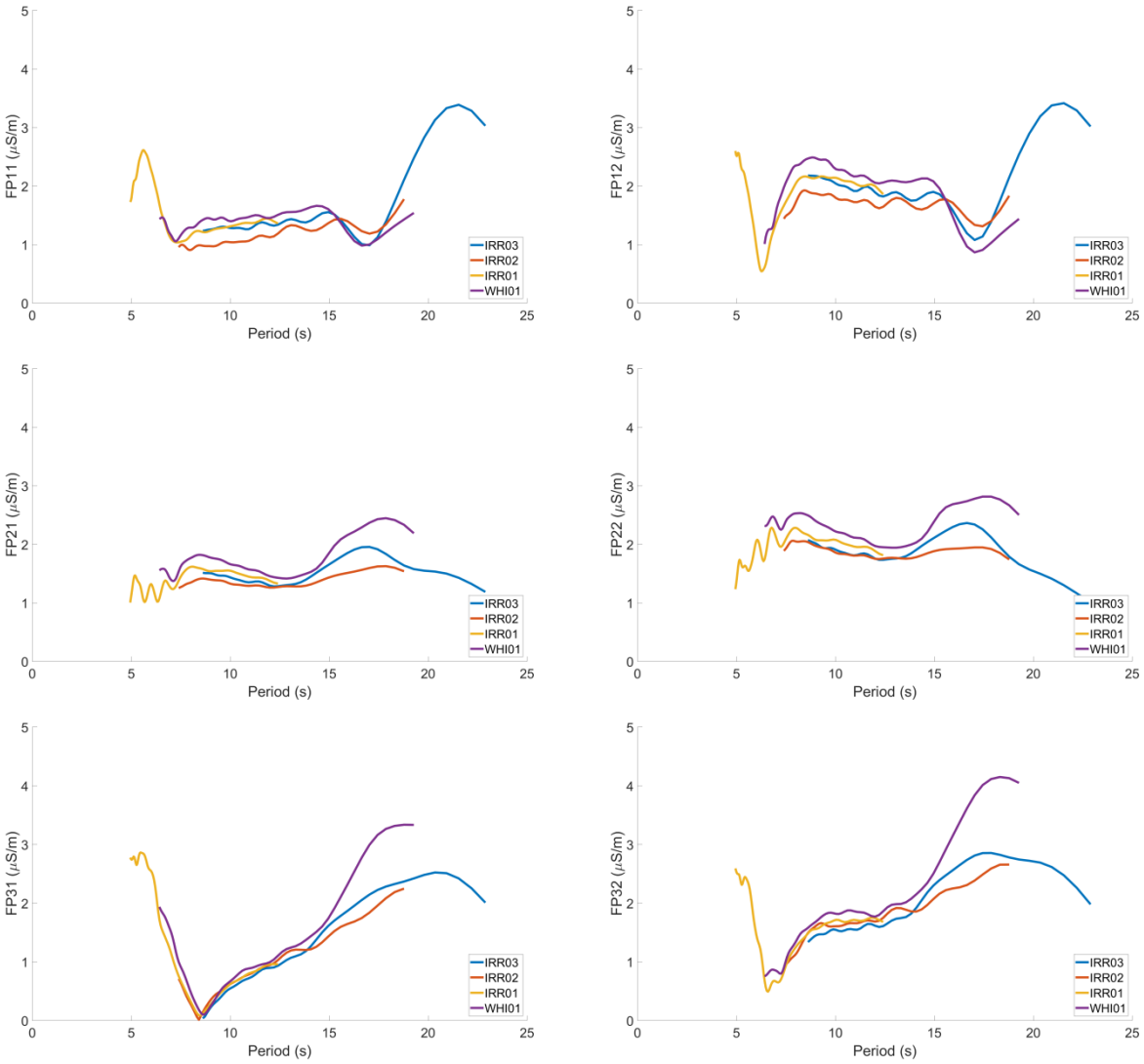

Figure 19: Strain at the selected points of the pontoons for a wave direction of 195°

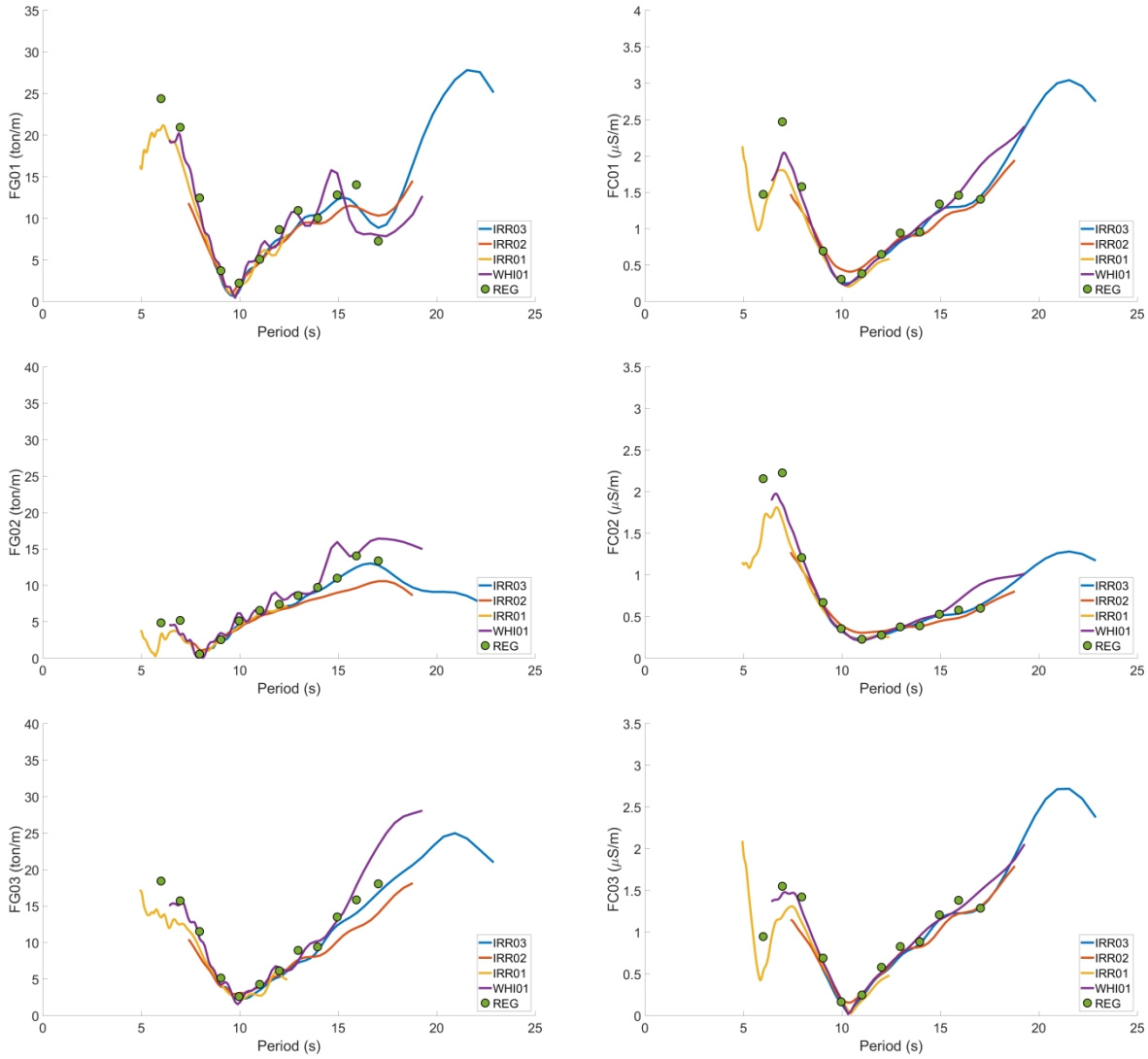

Figure 20: Tension at guy wires and tower bottom strain for a wave direction of 210°

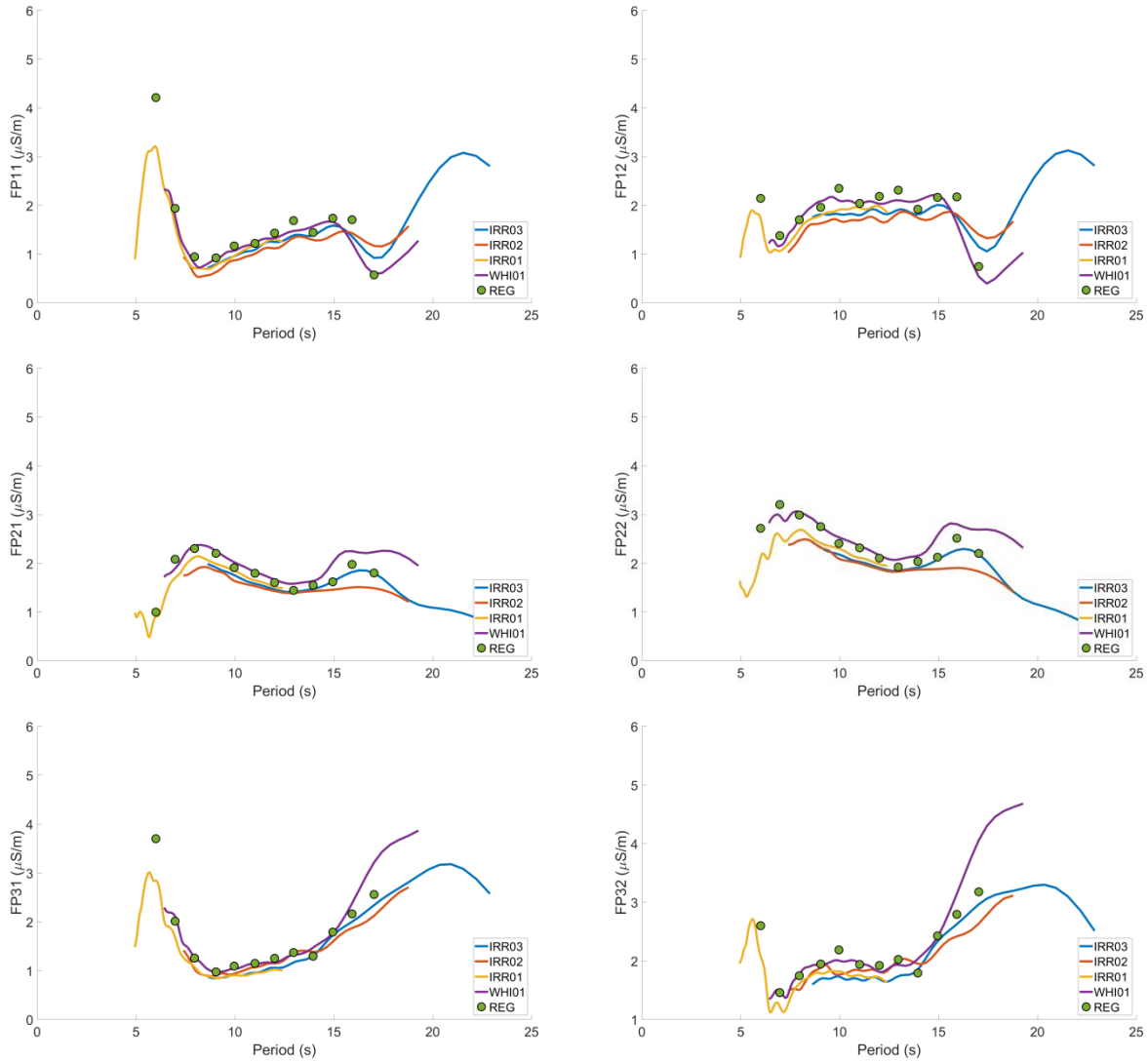

Figure 21: Strain at the selected points of the pontoons for a wave direction of 210°

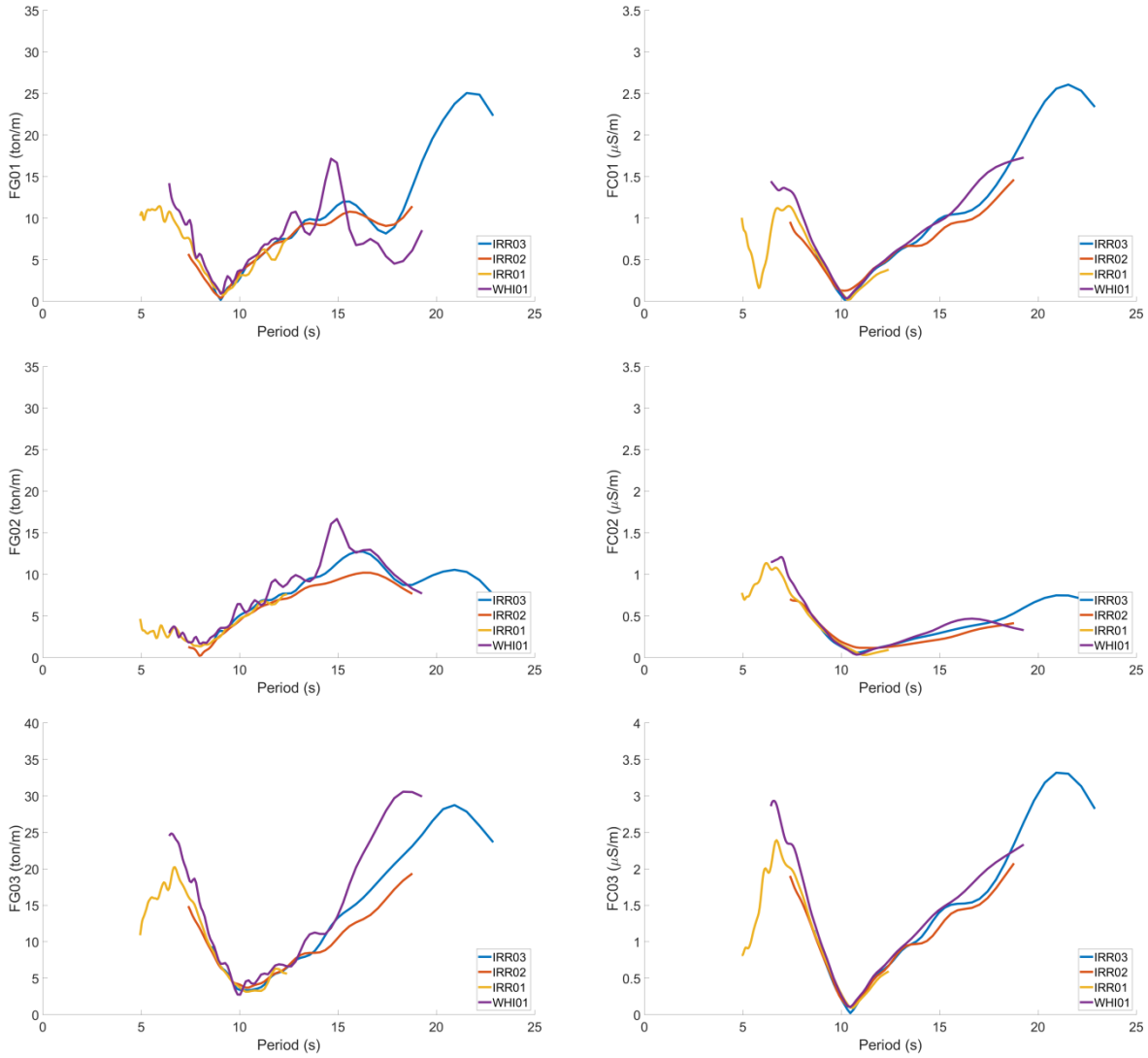

Figure 22: Tension at guy wires and tower bottom strain for a wave direction of 225°

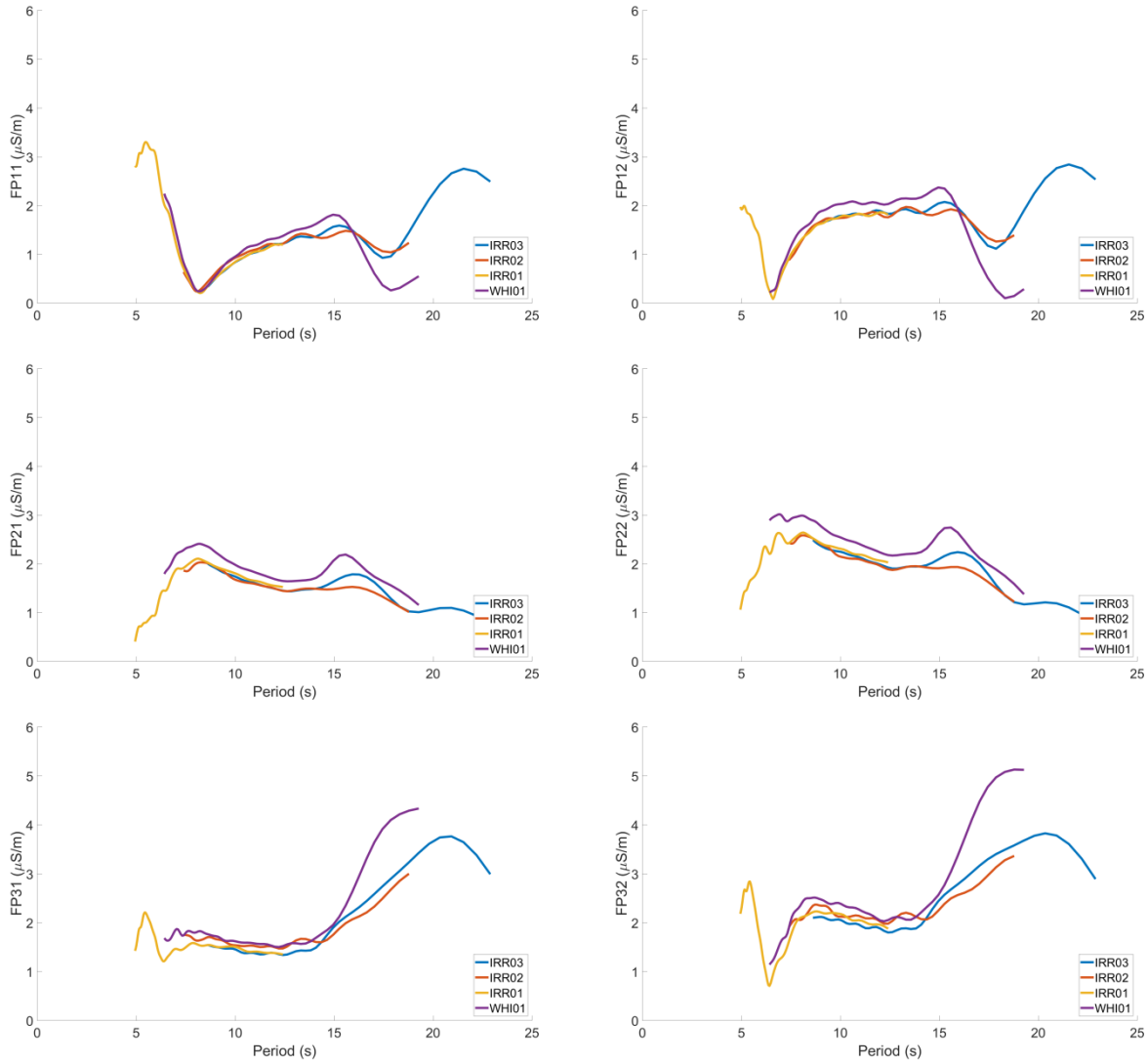

Figure 23: Strain at the selected points of the pontoons for a wave direction of 225°

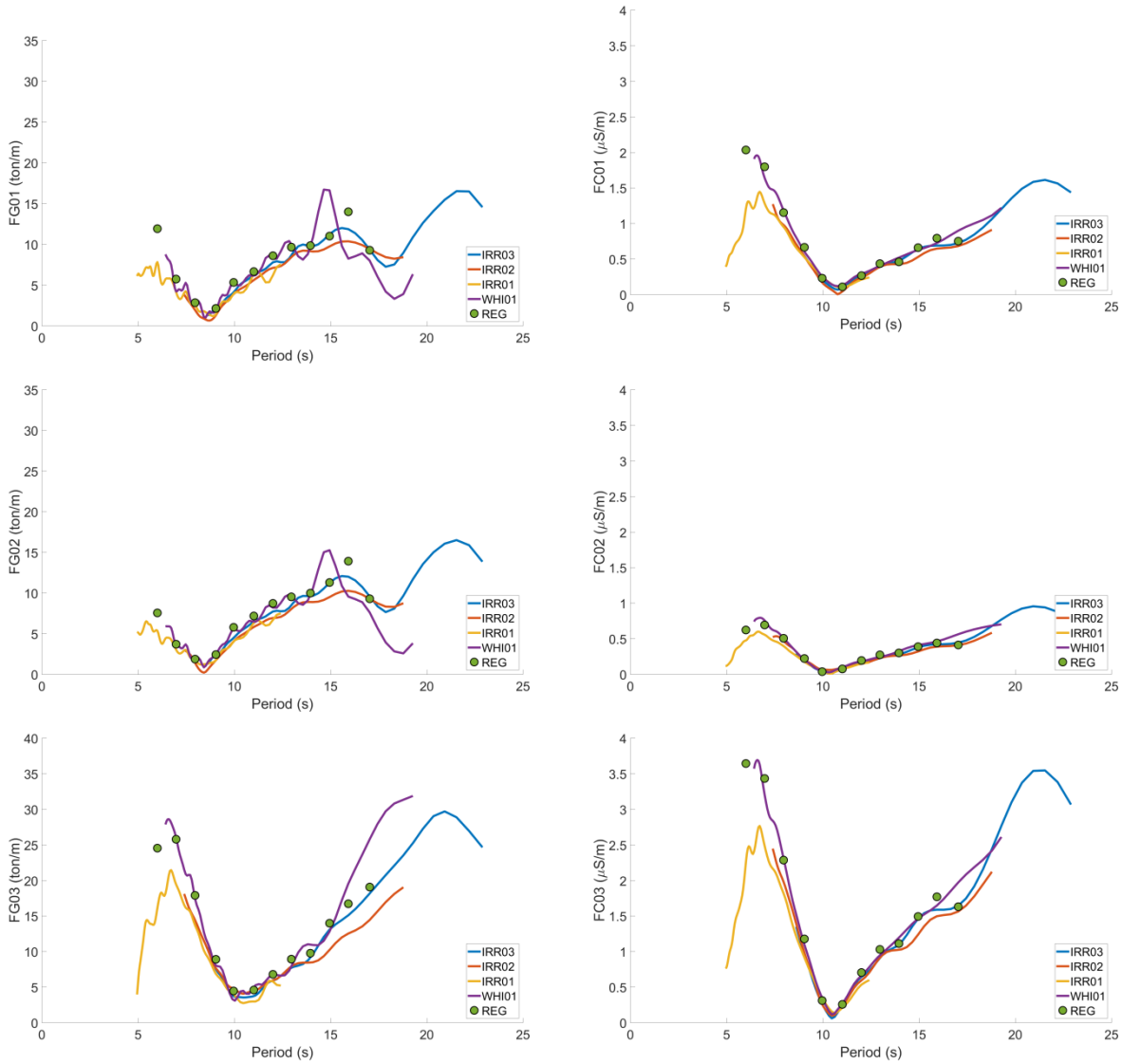

Figure 24: Tension at guy wires and tower bottom strain for a wave direction of 240°

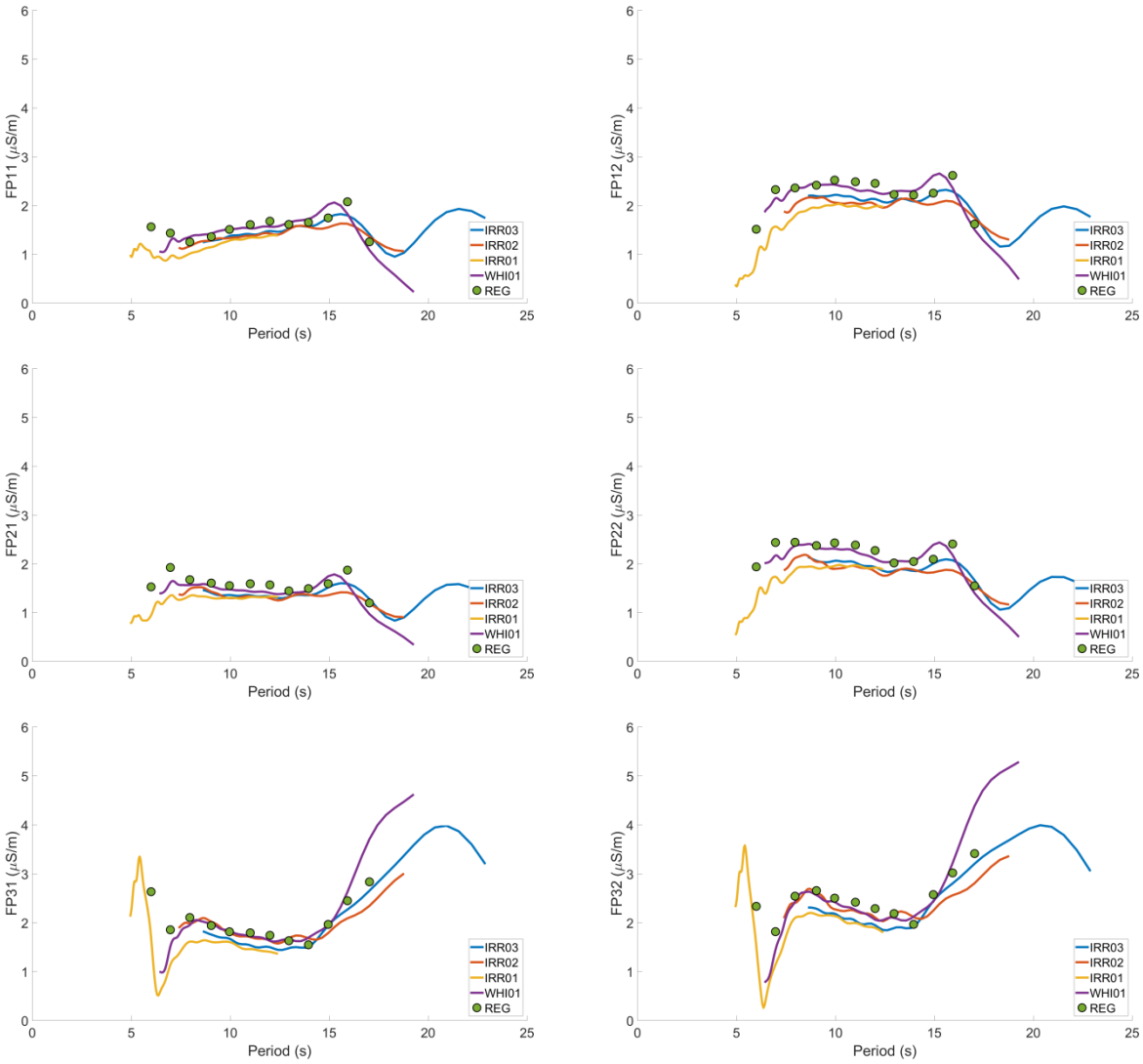

Figure 25: Strain at the selected points of the pontoons for a wave direction of 240°